CHEMISTRY OF MATERIALS
Cite This: Chem. Mater. 2019, 31, 1450−1459
Article
pubs.acs.org/cm

Tunable and Efficient Red to Near-Infrared Photoluminescence by Synergistic Exploitation of Core and Surface Silver Doping of CdSe Nanoplatelets

Ali Hossain Khan,[†,‡] Valerio Pinchetti,[§] Ivo Tanghe,[†,∥,⊥] Zhiya Dang,[‡] Beatriz Martín-García,[‡] Zeger Hens,[†,⊥] Dries Van Thourhout,[∥,⊥] Pieter Geiregat,[†,⊥] Sergio Brovelli,[§] and Iwan Moreels*[,†,‡]

[†]Department of Chemistry, Ghent University, Krijgslaan 281-S3, 9000 Ghent, Belgium
[‡]Istituto Italiano di Tecnologia, via Morego 30, 16163 Genova, Italy
[§]Dipartimento di Scienza dei Materiali, Universitá degli Studi di Milano-Bicocca, Via Cozzi 55, 20125 Milano, Italy
[∥]Photonics Research Group, INTEC Department, Ghent University-IMEC, Technologiepark-Zwijnaarde 15, 9052 Zwijnaarde, Belgium
[⊥]Center for Nano- and Biophotonics (NB-Photonics), Ghent University, Technologiepark-Zwijnaarde 15, 9052 Zwijnaarde, Belgium

Supporting Information

ABSTRACT: We report on the synthesis of silver (Ag)-doped CdSe nanoplatelets (NPLs) via postsynthesis cation exchange, using silver acetate as the Ag precursor. High-resolution transmission electron microscopy and X-ray diffraction confirmed that the NPLs maintain their morphology and crystal structure after doping when executing the exchange under reduced temperature in an ice bath. Spectroelectrochemistry and transient absorption spectroscopy revealed that Ag^+ acts as an acceptor dopant. Ag doping results in an emission that is tunable from 609 to 880 nm, with a Stokes shift up to 1 eV and a photoluminescence quantum efficiency exceeding 50%. This is achieved by varying the Ag dopant concentration, which determines the hole energy level, and by controlling the electron energy level via quantum confinement in CdSe NPLs with varying core thickness or in CdSe/CdS core/shell NPLs. As highly fluorescent materials with a strongly suppressed emission reabsorption because of the large Stokes shift, Ag-doped colloidal two-dimensional NPLs offer new opportunities for the development of colloidal nanocrystal-based optoelectronic and photonic devices such as light-emitting diodes or luminescent solar concentrators.

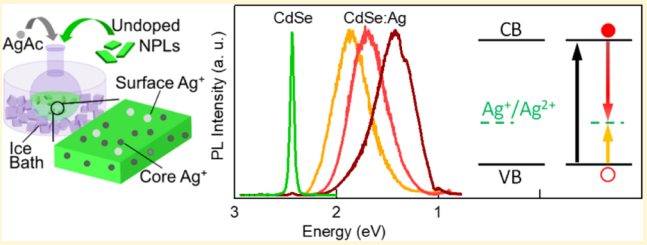

INTRODUCTION

Colloidal nanocrystals (NCs) are solution-processed nanomaterials that have tunable optoelectronic properties because of the size-dependent quantum confinement effect.[1,2] This enables efficient band-edge (BE) emission over a wide spectral range, from the ultraviolet to the near-infrared.[1] Continuous progress in the field has yielded NCs with diverse shapes, from spherical quantum dots (QDs), to anisotropic, radially confined nanorods, tetrapods, and octapods, and two-dimensional (2D) nanoplatelets (NPLs).[3] With shape control, one can precisely engineer the NC band structure and the associated optoelectronic properties such as the absorption cross section, the BE oscillator strength and exciton recombination time, the polarization of absorption and emission, and carrier relaxation dynamics in linear and nonlinear excitation regimes.[1,4]

Further band structure modifications occur when we include small amounts of dopants, capable of introducing atomic-like energy levels in the band gap of the host, which participate in the NC photophysics either as acceptor/donor states for excited carriers or as color centers sensitized by the NC matrix. In this way, the Stokes shift between the host absorption edge and the dopant-mediated emission is increased significantly, yielding bright NCs with a strongly reduced self-absorption.[5] Consequently, doped NCs have already been developed as potential candidates for application in luminescent solar concentrators (LSCs).[5−7] By localizing one or both charge carriers, the exciton lifetime is extended, as the electron−hole wave function overlap decreases. The long lifetime of the dopant emission, exceeding the typical biological background fluorescence, makes doped NCs convenient biosensing or bioimaging markers,[8] and in QD-sensitized solar cells it boosts the energy conversion efficiency.[9] In addition, charge-carrier localization can improve the single-photon emission character-

Received: December 27, 2018
Revised: January 29, 2019
Published: January 30, 2019

DOI: 10.1021/acs.chemmater.8b05334
Chem. Mater. 2019, 31, 1450−1459

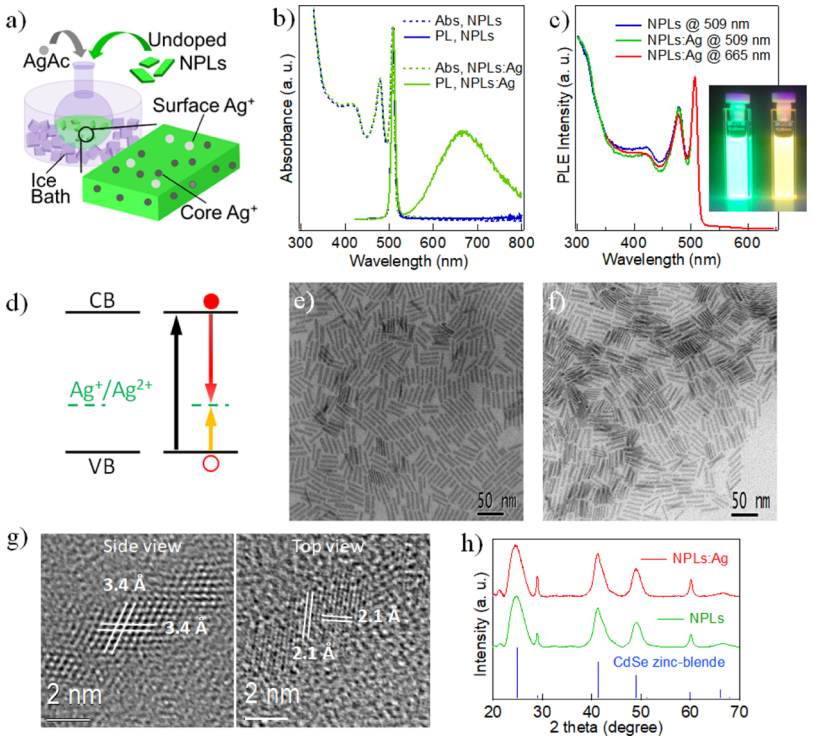

Figure 1. (a) Schematic representation of the cation exchange reaction, including the final CdSe:Ag NPLs. (b) Absorbance (dashed lines) and steady-state PL (solid lines) spectra of CdSe (blue) and CdSe:Ag NPLs (green), prepared by exposing the CdSe NPLs to silver acetate at a 0.2:1 Ag/Cd molar ratio. (c) PL excitation spectra of CdSe NPLs (blue) and CdSe:Ag NPLs measured at the BE (green) and dopant emission (red), respectively. The inset shows the images of the CdSe and CdSe:Ag NPL dispersions under UV illumination. (d) Schematic presentation of the relevant CdSe:Ag NPL energy levels. Black, yellow, and red arrows mark the photon absorption/electron−hole creation, hole relaxation into the Ag dopant, and electron−hole recombination process, respectively. (e−f) TEM images of the corresponding CdSe (e) and CdSe:Ag (f) NPLs. (g) HRTEM images, including a side view (left panel) and a top view (right panel) of the CdSe:Ag NPLs (prepared with an Ag/Cd ratio of 0.2:1). (h) XRD patterns of CdSe and CdSe:Ag NPLs. Vertical lines indicate bulk zinc-blende CdSe (ICDD card no. 98-018-6011).

istics of the extended 2D CdSe NPLs.[10] The broad dopant emission spectra make doped NCs potential candidates for multicolor or white light-emitting diodes (LEDs),[5,11,12] and, in the nonlinear emission regime, repulsive Coulomb interactions between multiple localized carriers in doped NCs yield a strongly blue-shifted biexciton emission,[13] which may lead to the realization of novel gain materials.

Isovalent doping of II−VI chalcogenide NCs, and more recently perovskite NCs, using manganese (Mn) has produced one of the most widely studied doped NC emitters.[5,7,14,15] Yet, Mn-doped NCs fluoresce over a limited spectral range (typically 580−620 nm), as the emission originates from localized *d-d* transitions.[14] Some tuning can be achieved by modifying the local crystal field around the dopant or by replacing the surface ligands.[16,17] Heterovalent or *electronic* NC doping with copper (Cu), on the other hand, yields a broader range (413−1100 nm has been reported),[5] as here only the holes are localized on the dopants, and the electron wave function remains delocalized over the entire NC and thus sensitive to quantum confinement. As Cu has two stable oxidation states, +1 and +2, there are different literature reports on its oxidation state in Cu-doped NCs.[5] An alternative electronic dopant in II−VI NCs is presented by silver (Ag), which, in contrast with Cu, remains in a +1 oxidation state as its second ionization potential is very high.[18] Photoexcitation leads to deep hole trapping at Ag^+ that subsequently forms Ag^{2+}, which acts as a radiative acceptor of a conduction band (CB) electron, resulting in a strong Stokes-shifted dopant emission.[19] As both the tetrahedral and octahedral ionic radii of Cd^{2+} (0.78 and 0.95 Å) are larger than those of Cu^+ (0.60 and 0.77 Å), yet smaller than those of Ag^+ (1.00 and 1.15 Å), for cadmium (Cd) chalcogenides Cu^+ could be either a substitutional or an interstitial impurity, whereas Ag^+ will form primarily substitutional impurities.[18,20,21] Also, the diffusion constant of Ag^+ is higher than that of Cu^+.[20] Ag^+ could therefore form an effective dopant in colloidal NCs, yet has, despite the recent successes in the doping of II−VI,[5,14] III−V,[20,22] and IV−VI[23] NCs, not received the same attention so far as Cu and Mn dopants.

In general, two methods are employed to incorporate Ag^+, either during synthesis of the host NCs[24] or by post-synthesis cation exchange.[18,20,21,25] The latter method separates doping from NC nucleation and growth, yielding more control over the doping level by the reaction time and the relative concentration of the added silver precursor. This strategy can also be employed in the opposite direction. Zhang et al. reported an inverted cation exchange reaction, mediated by ternary phosphines, to achieve CdS:Ag NCs, where they started with Ag_2S NCs and replaced the Ag^+ by Cd^{2+}.[26] A similar strategy also yielded CdSe:Ag QDs.[19]

With the recent development of a new class of colloidal NCs, 2D NPLs with uniform thickness and extended lateral dimensions, doping strategies can now be applied to these ultrathin semiconductor nanomaterials as well.[7,27] CdSe NPLs possess a high photoluminescence quantum efficiency (PL QE).[28−30] However, their emission typically displays a negligible Stokes shift, which can result in PL quenching in close-packed solid films. Therefore, CdSe:Ag NPLs could be

DOI: 10.1021/acs.chemmater.8b05334
Chem. Mater. 2019, 31, 1450−1459

Table 1. Ag Added to Synthesis, NPL Ag Concentration as Determined by ICP−OES, PL Peak Position (λ_{max}), fwhm and Average Lifetime (τ_{av}) of the BE (First Row) and Ag Emission (Subsequent Rows), Overall Emission QE (PL QE) and Relative Contribution of BE and Ag Emission, for the Different CdSe:Ag NPLs

Ag/Cd ratio added	Ag/Cd/Se (atom %)	λ_{max} (nm)	fwhm (meV)	τ_{av} (ns)	PL QE (%)	BE/Ag PL ratio (%:%)
0:1	0:58.3:41.7	509	43	5.3	51	
0.05:1	0.6:60.7:38.6	650	401	252	63	65:35
0.1:1	0.9:59.6:39.6	652	400	312	57	46:54
0.2:1	2.5:58.9:38.6	665	413	406	54	12:88
0.4:1	4.7:55.6:39.8	688	392	446	47	0.3:99.7
0.7:1	7.2:49.6:43.2	730	403	459	56	0.07:99.93
1:1	8.8:52.5:38.7	880	434	575		0.05:99.95

an excellent material for solid-state lighting[11,12,14] or other applications that require strongly reduced self-absorption, such as LSCs.[6,7,31] As an added advantage over colloidal QDs, the homogeneous thickness of NPLs results in a narrow emission spectrum,[32,33] which should permit to spectrally separate BE and dopant contributions, whereas the peculiar shape enhances the absorption cross section compared to spherical QDs[34] and yields anisotropic optical properties.[35−37] Despite this promise, no example of Ag-doped NPLs has been reported to date.

Here, we demonstrate the synthesis of CdSe:Ag NPLs via post-synthesis cation exchange under tempered conditions in an ice bath, using silver acetate as the Ag precursor. Transmission electron microscopy (TEM) and X-ray diffraction (XRD) revealed that the doped NPLs maintain the shape, size, and crystal structure of the parent NPLs. The Ag concentration can be tuned by the relative concentration of Ag precursors used, and we reached a maximal Ag concentration of 8.8% in the doped NPLs. Ag doping results in an emission that can be tuned from 609 to 880 nm, with a Stokes shift up to 372 nm (1 eV). This range is covered by varying the dopant concentration and by increasing the core thickness or growing CdSe/CdS hetero-NPLs. The smallest dopant concentration leads to a PL QE as high as 63%, and with an increased Ag concentration, the values remain around 45−55%.

RESULTS AND DISCUSSION

CdSe NPLs with a thickness of 4.5 monolayers (MLs) were first synthesized following a previously published procedure.[38] The purified NPLs were dispersed in hexane, and the concentration of NPLs was determined by the method reported by Achtstein et al.[34] The Cd atomic concentration was calculated from the number of CdSe units present per NPL (for 4.5 ML NPLs, a 1.36 nm thickness was taken), multiplied with the concentration of NPLs. Ag dopants were introduced via cation exchange reaction. In an initial series of experiments, the CdSe NPLs were mixed with different silver salt solutions (silver nitrate, silver trifluoroacetate) following standard procedures for colloidal NCs.[21,25] However, we observed that the NPLs were not stable under these conditions, likely because of the rapid cation exchange in the 1.36 nm thin NPLs (Supporting Information, Figure S1).

To avoid this, we resorted to silver acetate, which reacts more slowly, and we further reduced the reaction rate by performing the exchange around 0 °C in an ice bath (under ambient atmosphere, Figure 1a). In a typical reaction, we added silver acetate, in an Ag/Cd molar ratio of 0.2:1, to a solution of CdSe NPLs under continuous stirring. The reaction was allowed to proceed for 30 min. The absorbance and PL spectra of the resulting purified solution are presented in Figure 1b. After exchange, a broad peak with maximum at 665 nm appears in the PL spectrum next to the signature BE emission of the 4.5 ML NPLs at 509 nm. Note that the absorbance spectrum of the CdSe:Ag NPLs yields no particular features in the region of the broad PL peak. The PL excitation spectra of the CdSe:Ag NPLs, collected at the BE (509 nm) and the dopant (665 nm) emission wavelength, respectively, are largely superposed (Figure 1c), demonstrating that both the BE and dopant emission originate from absorption in the NPLs and confirming the incorporation of Ag into the NPLs. Under UV illumination (inset of Figure 1c), we can appreciate the bright yellow emission of the CdSe:Ag NPLs, compared to the green-emitting original NPLs. The schematics of the multistep recombination process leading to the dopant PL is depicted in Figure 1d, showing, after photoexcitation (step 1, black arrow), the initial capture of the excited valence band (VB) hole in Ag^+, following the reaction $Ag^+ + h^+ \rightarrow Ag^{2+}$ (step 2, orange arrow), and the subsequent radiative decay of the CB electron into the dopant center (step 3, red arrow), resulting in a Stokes-shifted emission and a concomitant reduction of the metastable Ag^{2+} site to its stable +1 ground-state configuration.[19]

TEM images of the CdSe NPLs show a rectangular shape with an average length of 28 ± 3 nm and a width of 3.7 ± 0.5 nm (Figure 1e). For the doped NPLs, we measured similar dimensions of 28 ± 4 nm by 3.7 ± 0.7 nm (Figure 1f), confirming that the cation exchange, performed under tempered conditions, does not modify the overall NPL size. High-resolution TEM (HRTEM) images of CdSe:Ag NPLs are presented in Figure 1g. Both the side- and top-view HRTEM images show that they are highly crystalline, with 3.4 and 2.1 Å *d*-spacings corresponding to the (111) and (220) planes of zinc-blende CdSe, comparable to other reported zinc-blende CdSe NPLs.[30,39] The XRD patterns (Figure 1h) confirm the HRTEM results. As the diffraction peaks occur at the same angles for CdSe (green pattern) and CdSe:Ag (red pattern, see also Supporting Information, Table S1), we can again conclude that no significant changes are imposed on the overall crystal structure after doping.

The relative concentration of silver acetate affects the Ag doping concentration in the final CdSe:Ag NPLs. We performed cation exchange reactions, exposing the CdSe NPLs for 30 min to silver acetate in an ice bath, with Ag/Cd molar ratios varying from 0.05:1 to 1:1, and we quantified the incorporation of Ag into the NPLs with inductively coupled plasma optical emission spectrometry (ICP−OES, Table 1). We observed a monotonic increase of the amount of Ag in the CdSe:Ag composition, eventually reaching 8.8%. Even at these concentrations, no variation of the NPL size and shape was observed (Supporting Information, Figure S2). From the CdSe NPL dimensions, 28 nm by 3.7 nm and a thickness of 1.36 nm,

DOI: 10.1021/acs.chemmater.8b05334
Chem. Mater. 2019, 31, 1450−1459

we estimated that the range of 0.6−8.8% Ag corresponds to about 30−440 atoms per NPL. Note that the ICP−OES data indicate that only about 10−15% of Ag present in solution is actually incorporated into the NPLs.

We also highlight that, at such high nominal doping levels, no undoped NPLs are statistically expected to be found in the ensemble. Therefore, the observation of residual BE PL in Figure 1b indicates that only a subset of the Ag dopants diffuses inside the NPLs and actively participates in the excitonic decay, whereas the remaining fraction of the Ag cations likely adsorbs onto the particle surface (see also the schematic in Figure 1a). Support for this interpretation is provided by the comparison between the absorption spectra of the undoped and doped NPLs. Specifically, independent of the Ag concentration, the normalized CdSe:Ag NPL absorption profiles show spectral features that match well with the original CdSe NPLs (Figure 2a). Below the CdSe BE, Ag-doped NPLs

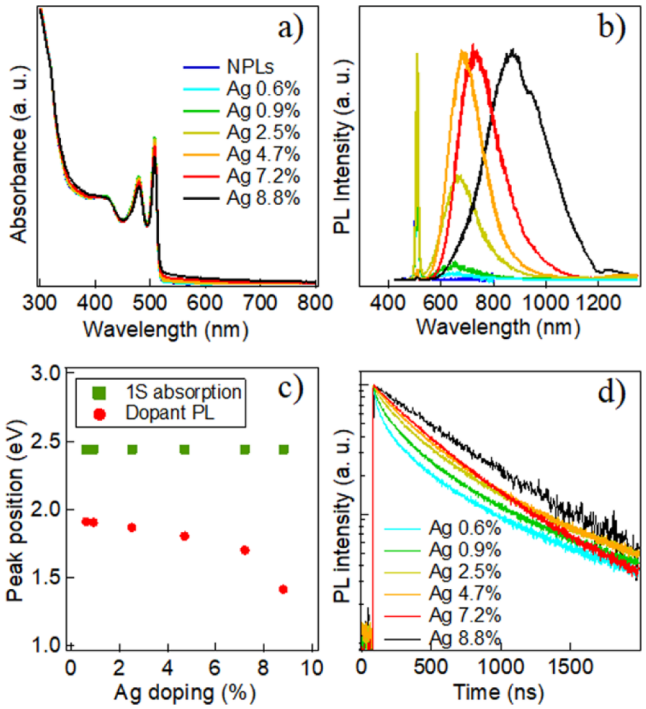

Figure 2. (a) UV−vis absorbance spectra of CdSe:Ag NPLs at increasing Ag concentration. (b) Corresponding steady-state PL spectra (λ_{ex} = 400 nm, same color labels as the absorbance spectra). (c) Plot of the PL peak position against Ag concentration, highlighting the red shift of the dopant emission (red dots), whereas the BE absorption remains fixed (green squares). (d) PL decay traces of the dopant emission for different doping concentrations.

exhibit a measurable, yet very weak absorption tail that can be associated with the direct absorption in Ag^+ centers, consistent with the recent observation in CdSe:Ag QDs,[19] where a clear absorption feature could be discerned. The weak subgap absorption intensity observed for our NPLs, despite the nominally comparable doping level, can be rationalized when considering the different preparation methods employed. In ref 19, CdSe:Ag NCs were obtained via an incomplete cation exchange reaction starting from Ag_2Se NCs, which enables to retain a large amount of Ag cations in the interior of the doped NCs. Here, on the other hand, Ag doping was achieved by exposing CdSe NPLs to silver acetate. The observed differences between the spectral features of the two Ag-doped CdSe nanostructures with comparable overall Ag concentration corroborate the picture that the current procedure leads to a larger fraction of surface-adsorbed Ag, and thus a lower concentration of Ag effectively incorporated into the CdSe lattice. This is also consistent with the previous results by Sahu et al.[21] and Morgan and Kelley[40] on CdSe QDs, Amit et al.[22] on InAs, and Kroupa et al.[23] on PbSe and with the spectroscopic and spectroelectrochemical (SEC) results reported in the following sections.

Looking closer at the absorption and PL spectra of doped NPLs as a function of the dopant concentration, we notice that the BE absorption peak remains fixed at 508 nm (2.44 eV, Figure 2a), whereas the spectral position of the dopant PL varies from 650 to 880 nm (1.41−1.91 eV, Figure 2b). The trends are quantified in Figure 2c as a function of the doping level. In the low-concentration limit, we obtained a Stokes shift of 0.53 eV, similar to the 0.4 eV measured by Nelson et al.[18] and Pinchetti et al.[19] in CdSe QDs. At a higher concentration, the Stokes shift increases up to 1.03 eV. Although the dopant emission has a nearly constant full width at half-maximum (fwhm) of 0.39−0.43 eV (Table 1), broadened by strong phonon coupling[18] and a possible distribution of Ag concentrations across the NPL ensemble, an efficient spectral separation of the BE and dopant features is still obtained, assisted by the 9 nm (45 meV) narrow fwhm (calculated by doubling the half width of the red edge of the absorption peak) of the NPL BE absorption. The fixed spectral position of the latter confirms that the electronic structure of the host NPLs is not affected by the inclusion of Ag dopants, even at a high concentration. On the other hand, the shifting dopant emission suggests that, with increasing Ag concentration, changes occur to the local energy levels of the dopants as the host goes from nearly pure CdSe to CdSe:Ag with 8.8% Ag, possibly because of the local crystal field modifications or small Ag_2Se cluster formation.[20,24,41] For comparison, 2 nm Ag_2Se QDs show emission with a PL maximum at 1030 nm.[42]

The Ag doping level is also found to modify the dynamics of the dopant-mediated PL. Specifically, the lightest doped CdSe:Ag NPLs exhibit a multiexponential decay (Figure 2d, Supporting Information Table S2) likely because of a distribution of decay pathways. Interestingly, upon increasing the doping level, this progressively turns into a single-exponential behavior that attests to an evolution toward a homogeneous doping of the CdSe:Ag NPL ensemble. As shown in Table 1, such a trend is accompanied by a gradual increase of the amplitude-averaged PL lifetime. For the heaviest doped NPLs, lifetimes are about a factor of 2 longer than that of CdSe:Ag QDs, which yielded 200 ns.[18,19] Hence, the smaller subgap absorption tail observed in Figure 2a is, next to the lower effective concentration of Ag inside the lattice compared to CdSe:Ag QDs, also caused by the weak lateral confinement regime in NPLs, leading to an electron that is bound to the localized hole only by Coulomb interactions, which may yield a reduced electron−hole overlap compared to QDs.

Remarkably, all samples display a high absolute PL QE, up to 63% for the smallest dopant concentration and evolving toward values around 45−55% when the Ag concentration is increased (Table 1). These PL QEs are comparable to undoped CdSe NPLs despite the significantly longer PL lifetimes (Figure 2d, Table 1), suggesting that carrier localization on the Ag dopants and surface passivation by the adsorbed Ag ions (as further confirmed by the SEC analysis

DOI: 10.1021/acs.chemmater.8b05334
Chem. Mater. 2019, 31, 1450−1459

reported below) lead to a suppression of the nonradiative recombination rate. Focusing further on the broad dopant emission, its relative intensity scales with the Ag concentration (Figure 2b, Table 1). Starting at 4.7% Ag concentration, more than 99% of the emission originates from the Ag dopant level, whereas samples with a lower Ag concentration maintain a finite contribution of BE PL. This supports the assumption that Ag is initially adsorbed on the NPL surface, whereas only at higher concentration they also become substitutional dopants and act as deep hole acceptor states.[18,40,41] The ratio of doped and undoped—or surface-decorated—NPLs can be quantified as follows. The initial CdSe NPLs have a PL QE of 51%, similar to the PL QE of the CdSe:Ag NPLs that display only dopant emission (samples with 4.7 and 7.2% Ag, yielding an average PL QE of 51.5%). When assuming that the PL QE of CdSe and CdSe:Ag NPLs does not vary significantly over the different samples, one can derive that the relative weight of the dopant emission directly represents the fraction of NPLs where Ag dopants are inserted into the CdSe lattice, and Table 1 hereby shows that the CdSe:Ag NPL samples with an Ag concentration below 4.7% maintain a distinct fraction of undoped NPLs in the ensemble. Nevertheless, the tunable PL spectra, combined with the minimal overlap between the absorption and PL spectra and the predominant contribution of the Ag dopant emission to the overall spectrum at larger Ag concentration, make CdSe:Ag NPLs attractive phosphors for optical imaging or down-conversion of blue or solar light in LEDs and LSCs, respectively.[5,8,31]

For a closer examination of the carrier dynamics in the CdSe:Ag NPLs, we investigated the hole relaxation process using transient absorption spectroscopy. As the CdSe:Ag NPLs have a nearly negligible Ag-related absorption band (Figure 2a), hole relaxation rates can no longer be derived directly from the buildup of Ag absorption, as was done previously on CdSe:Ag QDs.[19] Instead, we inferred this from the BE absorption using state-resolved transient absorption spectroscopy. This method has already been applied successfully to study carrier cooling, exciton−phonon coupling, and multiexciton interactions.[43]

Here, we excited the CdSe and CdSe:Ag NPLs at a wavelength resonant with the heavy hole exciton (HH-X) transition and monitored the bleach signal of the heavy hole (dark blue area) and light hole exciton (LH-X, light blue area) transitions (see Figure 3a,b). Importantly, both excitons are derived from the same CB state but from different VB states. Hence, the hole capture from the HH exciton will leave behind a single CB electron that will affect light absorption by both the HH-X and LH-X transitions. Electron capture, on the other hand, will leave behind a heavy hole, which should only affect light absorption by the HH-X transition. Experimentally, we found that the HH-X and LH-X bleach traces exhibit the same decay dynamics at longer delay times. This indicates that the HH exciton suffers from rapid hole capture, after which the decay of the remaining CB electron determines the bleach of the HH-X and LH-X absorbance. Consequently, when normalizing both traces at a long delay time (Figure 3c), and subtracting the former from the latter, one obtains the hole dynamics of the system (Figure 3d).

Fitting the resulting trace for CdSe NPLs (black curve) yields three time constants (Supporting Information, Table S3), reflecting a range of surface traps and associated decay constants, as for CdSe QDs.[44] The amplitude-averaged decay constant equals 23.5 ps. When constructing and fitting similar

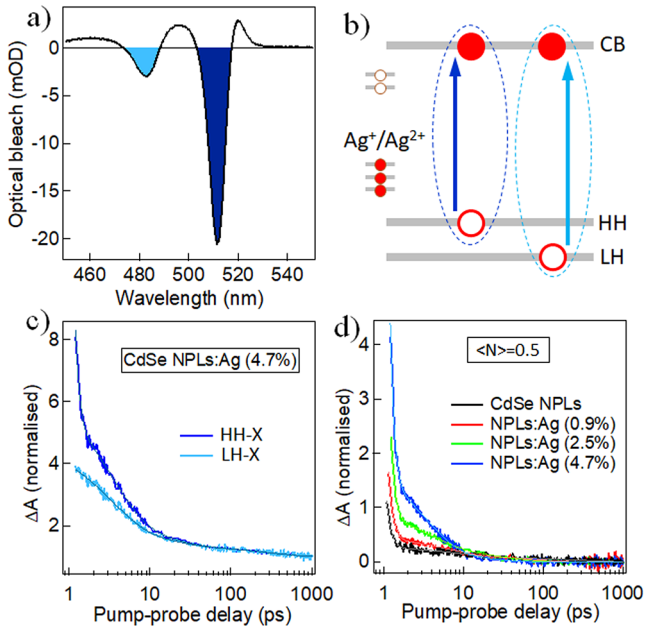

Figure 3. (a) Identification of the HH-X (dark blue) and LH-X (light blue) bands in the transient absorption spectra, which were used for the analysis of the hole dynamics. (b) Schematics illustrating the band structure of CdSe:Ag NPLs, including occupied and unoccupied surface states. (c) HH-X (dark blue) and LH-X (light blue) transient absorption traces (shown for the sample with 4.7% Ag). (d) Hole dynamics (HH trace subtracted with LH trace) for CdSe NPLs (black) and CdSe:Ag NPLs with 0.9% (red), 2.5% (green), and 4.7% (blue) Ag.

traces for CdSe:Ag NPLs with the Ag concentration of 0.9, 2.5, and 4.7%, respectively (Figure 3d), we observed a progressive decrease of the relaxation constant, from 6.5 ps down to 1.9 ps for the sample with the highest Ag concentration (where also 99% of the emission originates from the dopants). As the decay constant is significantly smaller than that for undoped CdSe, and similar to the one found in CdSe:Ag QDs,[19] we can ascribe it to hole relaxation into the Ag dopant. Note that the ultrafast relaxation should lead to a complete quenching of BE PL, again corroborating that, at low Ag concentrations, we have a heterogeneous NPL ensemble, and only when exposing it to sufficiently high concentrations of Ag precursors, all NPLs are Ag-doped.

The ultrafast decay into the Ag^+ dopant level together with the surface passivation effect posited by the surface-adsorbed Ag atoms also modifies the interaction of charge carriers with surface defects. To shed light onto this mechanism and to clarify the nature of the intragap dopant state, we performed SEC experiments on CdSe:Ag NPLs with an Ag concentration of 2.5%. In these experiments, the NPLs are excited with a UV laser, and PL is collected while the position of the Fermi level (FL) is tuned by the application of an EC potential (V_{EC}). Specifically, a negative V_{EC} corresponds to the raising of the FL and leads to passivation of electron-poor surface states acting as nonradiative traps for the photogenerated CB electrons. Concomitantly, the excess electrons accumulated in the surface defects become efficient traps for the photogenerated VB holes. Conversely, a positive V_{EC} (corresponding to lowering the FL) depletes the NPL of the photoexcited electrons and concomitantly passivates the electron-rich defect states acting as efficient hole traps. The effect of V_{EC} on the emission efficiency of the NPLs is therefore determined by the

DOI: 10.1021/acs.chemmater.8b05334
Chem. Mater. 2019, 31, 1450−1459

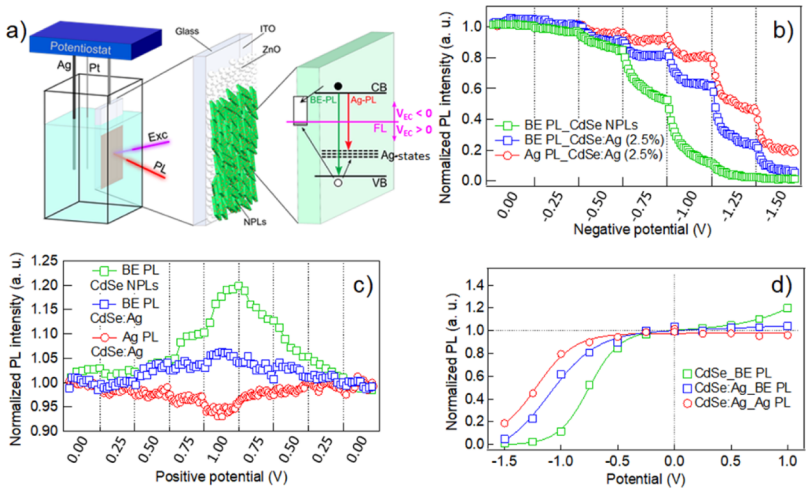

Figure 4. (a) Schematic depiction of the custom SEC setup consisting of an EC cell with $TBAClO_4$ in propylene carbonate (0.1 M) as an electrolyte and a working electrode comprising of an ITO-coated glass slide covered with a layer of ZnO nanoparticles (NPs) and CdSe:Ag NPLs. Also shown is the radiative recombination pathway (red arrow) of photoexcited CB electrons to the intragap Ag state following the capture of the VB hole (black arrow). The green arrow indicates the BE radiative recombination. Competitive nonradiative carrier trapping processes to defect states are shown by black arrows. FL is indicated by a pink line. (b-c) SEC measurements on CdSe and CdSe:Ag NPLs at negative (b) and positive (c) bias V_{EC}. The evolution of the PL intensity after each potential step indicates a slow charging/decharging of the NPL film. (d) PL intensity as a function of V_{EC} for CdSe NPLs (green squares), and the BE emission (blue squares) and Ag emission (red circles) of CdSe:Ag NPLs. Data were taken from the final values in panels (b,c), just before a subsequent potential step was applied.

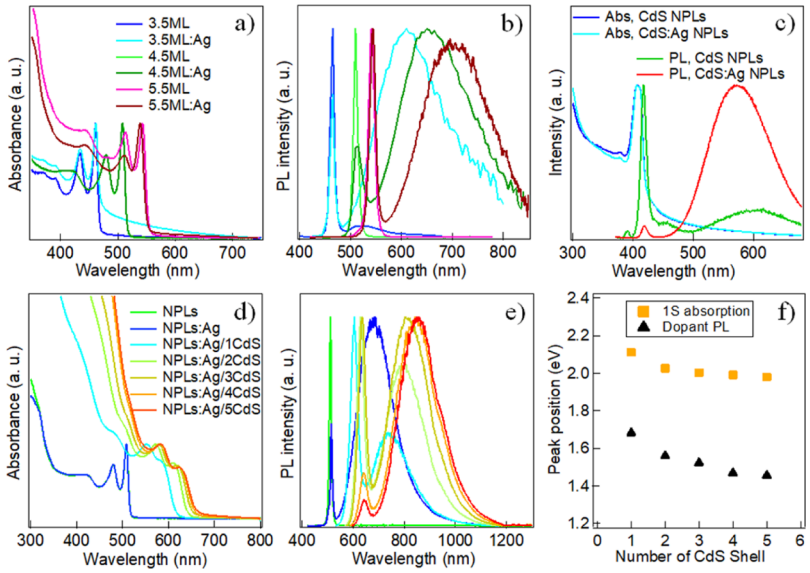

Figure 5. (a) Absorption and (b) PL spectra of CdSe and CdSe:Ag NPLs with thicknesses of 3.5, 4.5, and 5.5 MLs. (c) Absorption and PL spectra of CdS and CdS:Ag NPLs. (d) Absorption and (e) PL spectra of 4.5 ML CdSe:Ag NPLs and the corresponding CdSe:Ag/CdS core−shell NPLs with different number of CdS MLs. (f) Change of the BE absorption and dopant PL peak positions with the number of CdS shell layers.

competition between the selective passivation/activation of carrier traps and their respective trapping rates and by the occupancy of the surface states at V_{EC} = 0 V.[45,46] For this reason, SEC measurements are an effective tool to determine the trapping mechanisms affecting the exciton decay. In the specific case of CdSe:Ag NPLs, the selectivity of SEC measurements for the BE carriers of different signs further allows us to probe the electronic nature of the intragap Ag state responsible for the observed photophysics. The custom SEC experimental setup is depicted in Figure 4a. Here, a working electrode composed of a thin film of NPLs dip-coated onto a ZnO-coated indium tin oxide (ITO) electrode is immersed into an electrolytic solution of tetrabutylammonium (0.1 M) in propylene carbonate. Figure 4a also depicts the band energy diagram of CdSe:Ag NPLs. According to a previous report,[19] the FL at V_{EC} = 0 V is placed between the intragap states of Ag^+ dopants because of the fully occupied *d*-orbitals (electronic configuration $4d^{10}$) and the host CB. Looking first at the undoped CdSe NPLs under a negative V_{EC}, we observe an almost complete PL quenching (Figure 4b). In contrast, the application of a positive EC potential leads to a PL brightening of ∼20% (Figure 4c). In agreement with a previous report,[45] these observations indicate that the major nonradiative recombination channel in undoped CdSe NPLs is hole trapping.

DOI: 10.1021/acs.chemmater.8b05334
Chem. Mater. 2019, 31, 1450−1459

Moving on to Ag-doped NPLs (2.5% Ag), Figure 4b,c reports the evolution of both the BE and the Ag-related emission intensities as a function of V_{EC}. Upon increasing the negative V_{EC}, we observe significant quenching of both emissions, although weaker compared to the undoped sample. Remarkably, at positive V_{EC}, the BE and Ag-related recombination channels show opposite trends: BE shows progressive brightening with increasing V_{EC} similar to the undoped sample, whereas Ag PL is quenched by ~5% (Figure 4c). As the optical response of BE PL (arising from the subset of CdSe NPLs that only contain surface-adsorbed Ag) to the application of both negative and positive V_{EC} is less pronounced than that for the sample that was not exposed to Ag (Figure 4d), the SEC experiments corroborate the picture that some nonradiative surface hole traps in the doped NPLs are passivated by surface-adsorbed Ag ions. It is also worth noting that, despite the longer PL lifetime, in doped NPLs, the Ag emission is less affected by the negative EC potential than the BE emission (~95% vs ~80% quenching respectively, Figure 4d), suggesting that the holes localized at the intragap Ag states are efficiently shielded from the surface traps. This is also in agreement with the picture of Ag serving as a hole acceptor with its *d*-states lying close to the VB of CdSe, therefore introducing a competitive channel for the photogenerated holes to localization at the surface traps and to BE recombination.

Finally, to demonstrate that Ag doping of colloidal NPLs via cation exchange is a versatile method, we applied the same procedure to different core thicknesses and NPL compositions. First, 3.5 and 5.5 ML CdSe NPLs were prepared by standard protocols,[47] and we performed a cation exchange reaction (with Ag/Cd ratio of 0.2:1) as described above. The absorption and PL spectra of the CdSe and CdSe:Ag NPLs are presented in Figure 5a,b. The PL spectra indicate that the dopant PL can be tuned from 609 to 702 nm by increasing the thickness of the host NPLs from 3.5 to 5.5 ML. In contrast with the result obtained when varying the dopant concentration (Figure 2), here the red shift is controlled by a reduced quantum confinement of the (delocalized) first electron state, as evidenced by the similar shift of both BE absorption and dopant emission (Supporting Information, Figure S3). The procedure is also applicable to CdS NPLs[48] (Figure 5c). Ag doping of 4.5 ML CdS NPLs —that emit at 417 nm— leads to a broad PL band centered at 570 nm. Further tuning of the dopant emission can be achieved by growing a CdS shell around the CdSe:Ag NPLs, which we obtained with colloidal atomic layer deposition.[49] Changes in the absorption and PL spectra of 4.5 ML CdSe:Ag NPLs (2.5% Ag) are presented in Figure 5d,e. One ML of CdS shell already shifts the dopant emission to the near-infrared region, at 737 nm. Finally, four more additional layers yielded emission at 852 nm. The red shift of the dopant level can again be ascribed to the reduced confinement of the first electron state (Figure 5f).

CONCLUSIONS

We have prepared colloidal Ag-doped CdSe NPLs by partial cation exchange. At an Ag concentration of 4.7% or higher, a uniform doping is achieved, as shown by the absence of residual BE emission and the single exponential decay of the dopant emission. The SEC and transient absorption measurements reveal that Ag^+ acts as an acceptor dopant, with a hole trapping rate of 1.9−6.5 ps, depending on the doping concentration. The dopant PL can be tuned by changing either the Ag concentration or by modifying the electron confinement energy by changing the thickness of the host NPLs or by coating CdSe:Ag NPLs with a CdS shell. With a tunable emission ranging from orange (609 nm) to near-infrared (880 nm) wavelengths, large Stokes shifts resulting in a suppressed emission reabsorption, and PL QE values that exceed 50% and remain as high as the host NPLs, these fluorescent CdSe:Ag NPLs form an interesting addition to the class of colloidal 2D NC emitters, with potential applications in LSCs or light-emitting devices, where efficient emission needs to be combined with high transparency.

EXPERIMENTAL METHODS

Synthesis Materials. Cadmium nitrate tetrahydrate (99.997%), sodium myristate (≥99%), methanol (99.9%), octadecene (ODE; 90%), cadmium(II) acetate ($Cd(OAc)_2$; 99.995%), cadmium acetate dihydrate ($Cd(OAc)_2{\cdot}2H_2O$), oleic acid (90%), trioctylphosphine (TOP; 90%), hexane (≥95%), silver acetate (99.99%), *N*-methylformamide (NMF, 99%), acetonitrile (99.8%), toluene (99.8%), and ethanol (≥99.8%) were purchased from Sigma-Aldrich. Cadmium oxide (99.999%) and selenium powder (Se; 99.99%) were purchased from Strem Chemicals. Ammonium sulfide (20−24% aqueous solution) was purchased from Alfa Aesar. All chemicals were used without further purification. Silver acetate and Se were stored in a glovebox.

Preparation of Cadmium Myristate. Cadmium nitrate tetrahydrate (3 g) was dissolved in 200 mL of methanol. In another round-bottom flask, 5 g of sodium myristate was dissolved in 500 mL of methanol using sonication. The cadmium solution was then added dropwise to the myristate solution and stirred for 2 h at room temperature. The resulting precipitate of cadmium myristate was filtered and washed several times with methanol and was dried in a freeze dryer overnight.

Synthesis of 3.5 ML CdSe NPLs.[47] In a three-neck flask, 240 mg of $Cd(OAc)_2$, 150 μL of oleic acid, and 15 mL of ODE were degassed for over 1 h at 80 °C. Then, under argon flow, the flask was heated to 180 °C, and 150 μL of 1 M TOPSe was quickly injected. The reaction was stopped after 20 min, and 2 mL of oleic acid was added when the reaction was cooled to room temperature. Finally, the NPLs were centrifuged twice at 6000 rpm for 10 min with ethanol and were dispersed in hexane.

Synthesis of 4.5 ML CdSe NPLs.[38] In a three-neck flask, 180 mg of cadmium myristate, 30 mg of Se, and 15 mL of ODE were degassed for 1 h at 120 °C. Then, the flask was heated to 240 °C under argon flow. When the temperature reached 210 °C, 80 mg of $Cd(OAc)_2$ was quickly introduced. The solution was held at 240 °C for 8 min, and the reaction was then stopped. The temperature was reduced to 160 °C, and 2 mL of oleic acid was added. When the temperature of the reaction solution reached room temperature, 15 mL of hexane was added. The mixture was then centrifuged at 3000 rpm for 10 min. The precipitate containing the mixture of 3.5 and 4.5 ML NPLs was suspended in 30 mL of hexane. The resultant solution was centrifuged at 6000 rpm for 10 min to remove the 3.5 ML NPLs as the precipitant.

Synthesis of 5.5 ML CdSe NPLs.[47] In a three-neck flask, 170 mg of cadmium myristate and 15 mL of ODE were degassed for 1 h at room temperature. Then, under argon flow, the flask was heated to 245 °C, and 1 mL of 0.15 M Se−ODE (prepared by dissolving 12 mg of Se in 1 mL of ODE by sonication) was injected. After 30 s of reaction, 90 mg of $Cd(OAc)_2$ was introduced. The solution was held at 245 °C for 10 min, and the temperature was then reduced to arrest the growth. At 150 °C, 2 mL of oleic acid was added, followed by the addition of 15 mL of hexane at room temperature. The mixture was then centrifuged at 3000 for 10 min, and the precipitate containing the NPLs was suspended in 30 mL of hexane. To remove the by-products (3.5 and 4.5 ML CdSe NPLs), few drops of acetonitrile were added and centrifuged at 6000 rpm for 30 min. The final decant contains the 5.5 ML CdSe NPLs.

DOI: 10.1021/acs.chemmater.8b05334
Chem. Mater. 2019, 31, 1450−1459

Silver Doping of CdSe NPLs. Taking the example of 4.5 ML NPLs, the concentration of cadmium ions in the NPL stock solution was calculated first by using the intrinsic absorption coefficient reported by Achtstein et al.[33] for 4.5 ML NPLs and the NPL dimensions as determined by TEM. The silver stock solution was prepared by dispersing silver acetate in hexane (1 mg/mL) in a glovebox. In a fixed amount of NPL solution, different volumes of silver stock solution were added to achieve different dopant concentrations. The reactions were performed in an ice bath for 30 min, under stirring in ambient atmosphere. Afterward, the unreacted silver salts were removed by centrifuging the suspension at 3000 rpm for 5 min. To dope other NPLs, the same procedure was adopted.

Synthesis of CdSe:Ag/CdS Core/shell NPLs. The NPLs were synthesized following the colloidal atomic layer deposition approach.[49] The first layer of sulfur was introduced by transferring the CdSe:Ag NPLs from hexane to 3 mL of NMF, to which 100 μL of ammonium sulfide (20% in water) was added. Afterward, the polar solution was isolated. A mixture of acetonitrile and toluene (1:4) was added to precipitate the NPLs. After centrifugation at 6000 rpm for 10 min, they were dispersed in 3 mL of NMF. This was repeated at least two times to remove the sulfur precursor from the solution. To grow the first layer of cadmium, 3 mL of 0.5 M cadmium acetate in NMF was introduced, and the suspension was stirred for 1 h. The NPLs were again purified as described above and dispersed in 3 mL of NMF. For thicker shells, the same procedure was repeated until the desirable thickness was reached. The final CdSe:Ag/CdS core/shell NPLs were dispersed in 3 mL of toluene with the addition of 250 μL of oleic acid to stabilize them in solution. The excess oleic acid was removed by precipitation of the NPLs with acetonitrile, followed by resuspension in hexane.

Synthesis of 4.5 ML CdS NPLs. The CdS NPLs were synthesized following the method of Li et al.[48] In a three-neck flask, 53 mg of cadmium acetate dehydrate, 1 mL of S−ODE solution (1.6 mg S per mL of ODE), 0.063 mL of oleic acid, and 5 mL of ODE were degassed with Ar at room temperature for 15 min, then heated to 260 °C under Ar flow, and kept under 260 °C for 1 min. Afterward, the reaction flask was slowly cooled, and at 160 °C, 1 mL of oleic acid was added. An excess of hexane was added, and the suspension was centrifuged at 6000 rpm for 10 min. The precipitate was suspended in hexane.

Elemental Analysis. For ICP−OES measurements, the doped NPLs were precipitated by adding excess acetonitrile and centrifuging at 6000 rpm for 10 min, and finally they were suspended in hexane. ICP−OES measurements were performed on an aiCAP 6000 spectrometer (Thermo Scientific). The NPLs were digested in aqua regia overnight prior to the measurements.

Transmission Electron Microscopy. The samples were purified once more by adding excess acetonitrile, centrifuging at 6000 rpm for 10 min, and suspending in hexane, followed by drop-casting a dilute suspension onto carbon-coated copper grids. TEM images were acquired on a JEOL JEM-1011 microscope equipped with a thermionic gun operated at an accelerating voltage of 100 kV. HRTEM measurements were carried out on a JEOL JEM-2200FS microscope equipped with a Schottky emitter operated at 200 kV, a CEOS spherical aberration corrector for the objective lens, and an in-column energy filter (Omega-type).

XRD Measurements. The XRD patterns were measured on a PANanalytical Empyrean X-ray diffractometer equipped with a 1.8 kW Cu Kα ceramic X-ray tube and a PIXcel^{3D} 2 × 2 area detector operating at 45 kV and 40 mA. Samples for the XRD measurements were prepared by drop-casting a concentrated NPL dispersion onto a miscut silicon substrate. The diffraction patterns were collected using a parallel-beam geometry and symmetric reflection mode.

Optical Characterization. Absorbance spectra of the NPLs in hexane were recorded using a Varian Cary 5000 UV−vis−NIR spectrophotometer. Steady-state and time-resolved PL spectra were measured using an Edinburgh Instruments FLS920 spectrofluorometer. The steady-state PL was collected by exciting the samples at 400 nm with a xenon lamp. The same setup coupled to an integrating sphere was used for PL QE measurements. The PL decay traces were recorded by exciting the samples at 405 nm using a 50 ps laser diode at a repetition rate of 0.05−1 MHz.

Transient Absorption Spectroscopy. The samples were excited using 110 fs pump pulses at the spectral position of the HH-X transition (510 nm), which were created from the 800 nm fundamental (Spitfire Ace, Spectra Physics) through a nonlinear conversion in an optical parametric amplifier (Light Conversion TOPAS). Equally short probe pulses were generated in a thin CaF_2 crystal using the 800 nm fundamental. The pulses were delayed relative to the pump using a mechanical delay stage. The probe spectrum in our experiments covered the UV−vis window from 350 nm up to 750 nm; yet, we focused our attention on the region near the BE, that is, the HH-X and LH-X transitions. To calculate the average number of absorbed photons $\langle N \rangle$ per platelet, we used the relation: $\langle N \rangle = J_{ph} \times \sigma$, where σ is the absorption cross section and J_{ph} is the photon flux. The flux was calculated from the average excitation power (0.1 mW), the repetition rate (500 Hz), and the beam area (0.029 cm^2). The cross section was calculated as 3.0×10^{-14} cm^2 at 510 nm, using the method of Achtstein et al.,[34] taking the specific NPL dimensions into account. The data shown was obtained at $\langle N \rangle = 0.5$.

Spectroelectrochemistry. ITO-coated glass slides (50 × 7 × 0.7 mm, R_S < 100 Ω) were purchased from Delta Technologies (part no. CG-90IN-CUV). The ITO-coated surface was first covered with zinc oxide (ZnO) NPs (Nanograde, ∼50 nm diameter) to avoid NPL emission quenching by fast charge/energy transfer to ITO. The ZnO NP layer (∼60 nm thick, as measured using a Dektak profilometer) was deposited by dip coating the glass/ITO substrate into an ethanol suspension of ZnO NPs (2 mg/mL, one dip for 10 s) and annealing at 150 °C for 10 min in a nitrogen glovebox. To test the stability of the glass/ITO/ZnO NP substrates during potential scans, we performed control experiments in which we monitored the changes in the optical absorption spectra for prolonged exposures to negative and positive potentials. The results of these measurements indicate that the substrates are unaffected by either positive or negative EC potentials for the exposure times of tens of minutes, which are much longer than the measurement time used in our SEC experiments (∼10 min). The NPLs were deposited onto the ZnO NP layer as a film of few MLs by dip coating from a dilute hexane solution. The ITO was connected as a working electrode to the potentiostat (BioLogic SP-200 research grade potentiostat/galvanostat), and the film was placed into a quartz cuvette filled with the electrolyte (0.1 M tetrabutylammonium perchlorate in propylene carbonate). Silver and platinum wires were used as the quasi-reference and counter electrodes, respectively. All potentials reported in this work are measured relative to the quasi-reference silver electrode during the staircase voltammetry scans (360 s per scan, 60 s per potential step). The film was excited at 3.06 eV with an EPL 405 (Edinburgh Inst.) 40 ps pulsed diode laser, and the emitted light was collected with a focusing lens and sent to a spectrometer coupled to a TM-C10083CA Hamamatsu minispectrometer.

■ ASSOCIATED CONTENT

Supporting Information

The Supporting Information is available free of charge on the ACS Publications website at DOI: 10.1021/acs.chemmater.8b05334.

Experimental methods, additional TEM images, XRD peak values and lattice constants, decay components of time-resolved fluorescence and transient absorption traces, and additional data for CdSe:Ag NPLs with different thicknesses (PDF)

■ AUTHOR INFORMATION

Corresponding Author

*E-mail: iwan.moreels@ugent.be.

DOI: 10.1021/acs.chemmater.8b05334
Chem. Mater. 2019, 31, 1450−1459

ORCID

Ali Hossain Khan: 0000-0001-7155-0200
Valerio Pinchetti: 0000-0003-3792-3661
Zeger Hens: 0000-0002-7041-3375
Pieter Geiregat: 0000-0001-7217-8738
Sergio Brovelli: 0000-0002-5993-855X
Iwan Moreels: 0000-0003-3998-7618

Author Contributions

The manuscript was written through contributions of all authors. All authors have given approval to the final version of the manuscript.

Notes

The authors declare no competing financial interest.

■ ACKNOWLEDGMENTS

Z.H., D.V.T., and I.T. acknowledge the Research Foundation Flanders (project 17006602). P.G. acknowledges the FWO-Vlaanderen for a Postdoctoral Fellowship. I.M. and Z.H. acknowledge Ghent University for funding (GOA 01G01019). This project has also received funding from the European Union's Horizon 2020 research and innovation program (grant agreement no. 696656 GrapheneCore1) and the European Research Council (ERC, grant agreement no. 714876 PHOCONA). V.P. and S.B. are grateful to the MIUR "Dipartimenti di Eccellenza 2017 Project—Materials for Energy".

■ REFERENCES

(1) Pietryga, J. M.; et al. Spectroscopic and Device Aspects of Nanocrystal Quantum Dots. *Chem. Rev.* **2016**, *116*, 10513−10622.
(2) Kovalenko, M. V.; et al. Prospects of Nanoscience with Nanocrystals. *ACS Nano* **2015**, *9*, 1012−1057.
(3) Talapin, D. V.; Lee, J.-S.; Kovalenko, M. V.; Shevchenko, E. V. Prospects of Colloidal Nanocrystals for Electronic and Optoelectronic Applications. *Chem. Rev.* **2010**, *110*, 389−458.
(4) Li, Q.; Lian, T. Area- and Thickness-Dependent Biexciton Auger Recombination in Colloidal CdSe Nanoplatelets: Breaking the "Universal Volume Scaling Law". *Nano Lett.* **2017**, *17*, 3152−3158.
(5) Knowles, K. E.; et al. Luminescent Colloidal Semiconductor Nanocrystals Containing Copper: Synthesis, Photophysics, and Applications. *Chem. Rev.* **2016**, *116*, 10820−10851.
(6) Bradshaw, L. R.; Knowles, K. E.; McDowall, S.; Gamelin, D. R. Nanocrystals for Luminescent Solar Concentrators. *Nano Lett.* **2015**, *15*, 1315−1323.
(7) Sharma, M.; et al. Near-Unity Emitting Copper-Doped Colloidal Semiconductor Quantum Wells for Luminescent Solar Concentrators. *Adv. Mater.* **2017**, *29*, 1700821.
(8) Wu, P.; Yan, X.-P. Doped Quantum Dots for Chemo/Biosensing and Bioimaging. *Chem. Soc. Rev.* **2013**, *42*, 5489−5521.
(9) Santra, P. K.; Kamat, P. V. Mn-Doped Quantum Dot Sensitized Solar Cells: a Strategy to Boost Efficiency over 5%. *J. Am. Chem. Soc.* **2012**, *134*, 2508−2511.
(10) Tenne, R.; et al. From Dilute Isovalent Substitution to Alloying in CdSeTe Nanoplatelets. *Phys. Chem. Chem. Phys.* **2016**, *18*, 15295−15303.
(11) Khan, A. H.; et al. Efficient Solid-State Light-Emitting CuCdS Nanocrystals Synthesized in Air. *Angew. Chem., Int. Ed.* **2015**, *54*, 2643−2648.
(12) Zhang, Z.; et al. Dual Emissive Cu:InP/ZnS/InP/ZnS Nanocrystals: Single-Source "Greener" Emitters with Flexibly Tunable Emission from Visible to Near-Infrared and Their Application in White Light-Emitting Diodes. *Chem. Mater.* **2015**, *27*, 1405−1411.
(13) Avidan, A.; Oron, D. Large Blue Shift of the Biexciton State in Tellurium Doped CdSe Colloidal Quantum Dots. *Nano Lett.* **2008**, *8*, 2384−2387.
(14) Pradhan, N.; Sarma, D. D. Advances in Light-Emitting Doped Semiconductor Nanocrystals. *J. Phys. Chem. Lett.* **2011**, *2*, 2818−2826.
(15) Meinardi, F.; et al. Doped Halide Perovskite Nanocrystals for Reabsorption-Free Luminescent Solar Concentrators. *ACS Energy Lett.* **2017**, *2*, 2368−2377.
(16) Hazarika, A.; Pandey, A.; Sarma, D. D. Rainbow Emission from an Atomic Transition in Doped Quantum Dots. *J. Phys. Chem. Lett.* **2014**, *5*, 2208−2213.
(17) Pradhan, N.; Peng, X. Efficient and Color-Tunable Mn-Doped ZnSe Nanocrystal Emitters: Control of Optical Performance via Greener Synthetic Chemistry. *J. Am. Chem. Soc.* **2007**, *129*, 3339−3347.
(18) Nelson, H. D.; et al. Mid-Gap States and Normal vs Inverted Bonding in Luminescent Cu+- and Ag+-Doped CdSe Nanocrystals. *J. Am. Chem. Soc.* **2017**, *139*, 6411−6421.
(19) Pinchetti, V.; et al. Excitonic Pathway to Photoinduced Magnetism in Colloidal Nanocrystals with Nonmagnetic Dopants. *Nat. Nanotechnol.* **2018**, *13*, 145−151.
(20) Mocatta, D.; et al. Heavily Doped Semiconductor Nanocrystal Quantum Dots. *Science* **2011**, *332*, 77−81.
(21) Sahu, A.; et al. Electronic Impurity Doping in CdSe Nanocrystals. *Nano Lett.* **2012**, *12*, 2587−2594.
(22) Amit, Y.; Li, Y.; Frenkel, A. I.; Banin, U. From Impurity Doping to Metallic Growth in Diffusion Doping: Properties and Structure of Silver-Doped InAs Nanocrystals. *ACS Nano* **2015**, *9*, 10790−10800.
(23) Kroupa, D. M.; et al. Synthesis and Spectroscopy of Silver-Doped PbSe Quantum Dots. *J. Am. Chem. Soc.* **2017**, *139*, 10382−10394.
(24) Shen, Q.; Liu, Y.; Xu, J.; Meng, C.; Liu, X. Microwave Induced Center-Doping of Silver Ions in Aqueous CdS Nanocrystals with Tunable, Impurity and Visible Emission. *Chem. Commun.* **2010**, *46*, 5701−5703.
(25) Son, D. H.; Hughes, S. M.; Yin, Y.; Alivisatos, A. P. Cation Exchange Reactions in Ionic Nanocrystals. *Science* **2004**, *306*, 1009−1012.
(26) Liu, J.; Zhao, Q.; Liu, J.-L.; Wu, Y.-S.; Cheng, Y.; Ji, M.-W.; Qian, H.-M.; Hao, W.-C.; Zhang, L.-J.; Wei, X.-J.; Wang, S.-G.; Zhang, J.-T.; Du, Y.; Dou, S.-X.; Zhu, H.-S. Heterovalent-Doping-Enabled Efficient Dopant Luminescence and Controllable Electronic Impurity Via a New Strategy of Preparing II−VI Nanocrystals. *Adv. Mater.* **2015**, *27*, 2753−2761.
(27) Delikanli, S.; et al. Mn2+-Doped CdSe/CdS Core/Multishell Colloidal Quantum Wells Enabling Tunable Carrier-Dopant Exchange Interactions. *ACS Nano* **2015**, *9*, 12473−12479.
(28) Liu, Y.-H.; Wayman, V. L.; Gibbons, P. C.; Loomis, R. A.; Buhro, W. E. Origin of High Photoluminescence Efficiencies in CdSe Quantum Belts. *Nano Lett.* **2010**, *10*, 352−357.
(29) Tessier, M. D.; et al. Spectroscopy of Colloidal Semiconductor Core/Shell Nanoplatelets with High Quantum Yield. *Nano Lett.* **2013**, *13*, 3321−3328.
(30) Polovitsyn, A.; et al. Synthesis of Air-Stable CdSe/ZnS Core−Shell Nanoplatelets with Tunable Emission Wavelength. *Chem. Mater.* **2017**, *29*, 5671−5680.
(31) Meinardi, F.; et al. Highly Efficient Large-Area Colourless Luminescent Solar Concentrators Using Heavy-Metal-Free Colloidal Quantum Dots. *Nat. Nanotechnol.* **2015**, *10*, 878−885.
(32) Tessier, M. D.; Javaux, C.; Maksimovic, I.; Loriette, V.; Dubertret, B. Spectroscopy of Single CdSe Nanoplatelets. *ACS Nano* **2012**, *6*, 6751−6758.
(33) Khan, A. H.; et al. Near-Infrared Emitting Colloidal PbS Nanoplatelets: Lateral Size Control and Optical Spectroscopy. *Chem. Mater.* **2017**, *29*, 2883−2889.
(34) Achtstein, A. W.; et al. Linear Absorption in CdSe Nanoplates: Thickness and Lateral Size Dependency of the Intrinsic Absorption. *J. Phys. Chem. C* **2015**, *119*, 20156−20161.
(35) Gao, Y.; Weidman, M. C.; Tisdale, W. A. CdSe Nanoplatelet Films with Controlled Orientation of their Transition Dipole Moment. *Nano Lett.* **2017**, *17*, 3837−3843.

DOI: 10.1021/acs.chemmater.8b05334
Chem. Mater. 2019, 31, 1450−1459

(36) Scott, R.; et al. Directed Emission of CdSe Nanoplatelets Originating From Strongly Anisotropic 2D Electronic Structure. *Nat. Nanotechnol.* **2017**, *12*, 1155−1160.
(37) Ma, X.; et al. Anisotropic Photoluminescence from Isotropic Optical Transition Dipoles in Semiconductor Nanoplatelets. *Nano Lett.* **2018**, *18*, 4647−4652.
(38) Bertrand, G. H. V.; Polovitsyn, A.; Christodoulou, S.; Hossain Khan, A.; Moreels, I. Shape Control of Zincblende CdSe Nanoplatelets. *Chem. Commun.* **2016**, *52*, 11975−11978.
(39) Christodoulou, S.; et al. Chloride-Induced Thickness Control in CdSe Nanoplatelets. *Nano Lett.* **2018**, *18*, 6248−6254.
(40) Morgan, D.; Kelley, D. F. Role of Surface States in Silver-Doped CdSe and CdSe/CdS Quantum Dots. *J. Phys. Chem. C* **2018**, *122*, 10627−10636.
(41) Ott, F. D.; Spiegel, L. L.; Norris, D. J.; Erwin, S. C. Microscopic Theory of Cation Exchange in CdSe Nanocrystals. *Phys. Rev. Lett.* **2014**, *113*, 156803.
(42) Yarema, M.; et al. Infrared Emitting and Photoconducting Colloidal Silver Chalcogenide Nanocrystal Quantum Dots from a Silylamide-Promoted Synthesis. *ACS Nano* **2011**, *5*, 3758−3765.
(43) Kambhampati, P. Unraveling the Structure and Dynamics of Excitons in Semiconductor Quantum Dots. *Acc. Chem. Res.* **2011**, *44*, 1−13.
(44) Califano, M.; Gómez-Campos, F. M. Universal Trapping Mechanism in Semiconductor Nanocrystals. *Nano Lett.* **2013**, *13*, 2047−2052.
(45) Lorenzon, M.; et al. Reversed Oxygen Sensing Using Colloidal Quantum Wells Towards Highly Emissive Photoresponsive Varnishes. *Nat. Commun.* **2015**, *6*, 6434.
(46) Brovelli, S.; Galland, C.; Viswanatha, R.; Klimov, V. I. Tuning Radiative Recombination in Cu-Doped Nanocrystals via Electrochemical Control of Surface Trapping. *Nano Lett.* **2012**, *12*, 4372−4379.
(47) She, C.; et al. Red, Yellow, Green, and Blue Amplified Spontaneous Emission and Lasing Using Colloidal CdSe Nanoplatelets. *ACS Nano* **2015**, *9*, 9475−9485.
(48) Li, Z.; et al. Uniform Thickness and Colloidal-Stable CdS Quantum Disks with Tunable Thickness: Synthesis and Properties. *Nano Res.* **2012**, *5*, 337−351.
(49) Ithurria, S.; Talapin, D. V. Colloidal Atomic Layer Deposition (c-ALD) using Self-Limiting Reactions at Nanocrystal Surface Coupled to Phase Transfer between Polar and Nonpolar Media. *J. Am. Chem. Soc.* **2012**, *134*, 18585−18590.

DOI: 10.1021/acs.chemmater.8b05334
Chem. Mater. 2019, 31, 1450−1459